2016 SCEC Annual Report: Tracking Seasonal Influences on Stress Changes and Predicted Seismicity Rates using Estimates of Anomalous Geodetic Strains in Southern California

Principal Investigator: William Holt

Institutional Affiliation: The Research Foundation of SUNY at Stony Brook University

1.0 Project Objectives

Quantifying transient tectonic signals continues to reveal new insights into fault behavior and crust/mantle rheology [*Segall and Matthews*, 1997; *McGuire and Segall*, 2003; *Freed and Bürgmann*, 2004; *Ji and Herring*, 2013**]**. Through previous SCEC funding we have developed, tested, and automated a geodetic network processing system for detection of anomalous strain transients in Southern California [*Holt and Shcherbenko*, 2013]. It is our goal to incorporate these into the Collaboratory for the Study of Earthquake Predictability (CSEP). The modeling procedure determines time-dependent displacement gradient fields from continuous GPS (cGPS) time series [*Hernandez et al*., 2005, 2007; *Holt and Shcherbenko*, 2013]. The method has been tested using the SCEC IV Transient Detection Exercise and is able to recover the spatial and temporal distribution of slow events and determine their statistical significance. To date we have detected several transient strain phenomena within southern California. We show that these anomalous strains have occurred on a variety of time scales, they involve heterogeneous distributions, and they have impacted stress rates and Coulomb stress changes on faults [*Shcherbenko*, 2014; *Shcherbenko and Holt*, 2015]. Current efforts are showing promise for quantifying links between measured strain changes, model stress changes, and seismicity rates. We applied the network processing tool in northern California where seasonal transient strains prior to the 2014 South Napa earthquake show a focused anomaly within the South Napa region [*Kraner et al*., 2017]. Using our time-dependent measurements obtained from the geodetic network processing tool [*Holt and Shcherbenko*, 2013] we are currently developing a data product that will enable the tracking of strain and stress change evolution, along with expected seismicity rate evolution through time. The work performed to date fulfills the SCEC Science Objective **5b** "*Application of geodetic detectors to the search for aseismic transients across southern California*" and also supports **2c, 1d**, and **1e** and **2d**. Moreover, this research fulfills the recommendations under **Research Strategies** in **Tectonic Geodesy** to: (a) "*Improve our understanding of the processes underlying detected transient deformation signals and/or their seismic hazard implications through data collection and development of new analysis tools*."

2.0 Method

Through previous SCEC support we have developed a geodetic network processing tool for quantifying transient deformation in southern California [*Holt and Shcherbenko*, 2013]. A pilot automated detection algorithm runs each day at Stony Brook and posts results to our lab computers and sends out an automated email summary each day. Estimates for anomalous strains for the last 24-hour time period are computed automatically and sent out each day. Estimates of the prior 2 weeks, 1 months, 3 months, 6 months, 1 year and 2 years anomalous strains are calculated automatically once a week. We are currently working issues so that it can be transferred over to run at the Collaboratory for the Study of Earthquake Predictability (CSEP) the way that it works at our home institution.

3.0 Results Obtained and Their Significance

3.1 Strain Transient Evolution and Estimates of Coulomb Stress Change on Faults

Analysis of the cGPS data have revealed significant transients on a variety of time scales. Some of these are linked with known earthquakes (post-seismic relaxation in El Mayor- Cucapah [*Pollitz et al*.,

2012]; Brawly Swarm, *Hauksson et al*., 2013), whereas others are linked with unknown, and potentially slow-slip, processes (Parkfield) (*Holt and Shcherbenko*, 2013), where tremor activity has been observed [*Shelly*, 2009, 2010]. We have investigated inferred stress changes on fault interfaces in association with the modeled strain tensor changes (Coulomb Stress Change) [*King et al*., 1992]. Target structure orientations for the Coulomb stress change calculations are the no-length change directions [*Holt and Haines*, 1993] in a steady state strain rate field (Figures 1a,b) determined from inversion [e.g., *Holt et al*., 2000a, 2000b; *Beavan and Haines*, 2001; Holt et al., 2010] of the SCEC4.0 velocity field [*Shen et al*., 2011], and most recently the UCERF3 GPS velocity field [*Field et al*., 2014]. Theoretical fault planes from the tensor solution (Figure 1b) are consistent with near-vertical dip in the vicinity of the major strike-slip structures. We assume continuity of surface strains down to the base of the seismogenic zone. In addition to using the no-length-change directions, we are also investigating the Coulomb stress changes using the UCERF3 model faults as target structures.

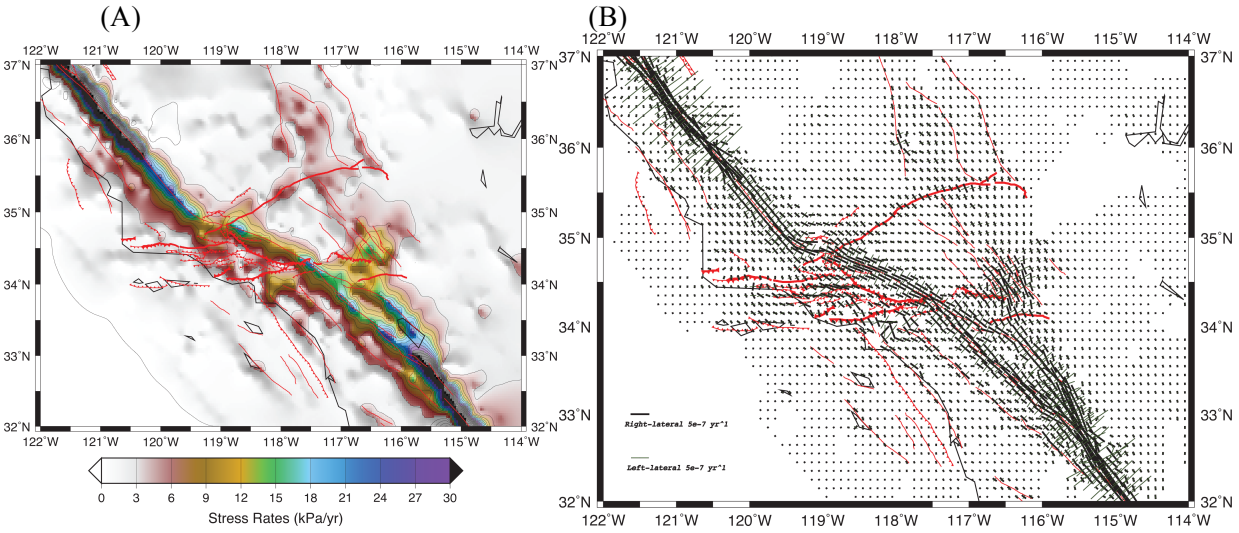

Figure 1. (A) Stress rates obtained from the steady-state strain rate tensor solution defined from SCEC4.0 velocity field [*Shen et al*., 2011]. We have assumed incompressible elastic [*Luttrell et al*., 2011] and the second invariant of the tensor field is plotted in (A). (B) No-length-change directions obtained from the steady-state strain rate tensor solution defined from SCEC4.0 velocity field (Bold lines = Right-lateral shear directions, light green lines = left-lateral shear direction).

3.2 Model Seismicity Rate Estimates

Using a rate/state algorithm [*Dieterich*, 1994; *Toda et al*., 2005] that incorporates the influence of all inferred Coulomb stress changes on faults (co-seismic and post-seismic) constrained by the cGPS data, we generate predicted seismicity rates and compare with observed rates for magnitudes > M 1.5. The background tectonic stressing rates come from the reference model (Figure 1), and background seismicity rates are determined by binning events of M>1.5 [*Hauksson et al*., 2012] within 0.1° x 0.1° sized grid areas. Seismicity rate patterns are well predicted throughout the regions affected in the far-field by the El Mayor-Cucapah event. We have found statistically significant increases in predicted model seismicity rates that match well with observations in the 3 years following the event [*Shcherbenko and Holt*, in preparation].

3.3 Sensitivity Tests

We have performed sensitivity tests to determine if the concentrations of strain anomalies near some of the faults are linked with the inhomogeneous and anisotropic variance-covariance weighting that we use in the inversion of cGPS observations for anomalous strains. The current weighting uses the geologic structures [*Jennings*, 1994; *Shen-Tu et al*., 1999] as information for probable orientation and relative magnitude of principal axes of model strains obtained in the inversion of cGPS displacements. This weighting introduces an *a priori* bias. Alternatively, we have experimented using a purely isotropic and

spatially homogeneous variance-covariance weighting in the inversion of the cGPS displacements. The model anomalous strain distributions were very close to that obtained using the anisotropic solution, suggesting that the model is not strongly dependent on the a priori information, and that model results depend primarily on the cGPS displacements [*Shcherbenko*, 2014; *Shcherbenko and Holt*, 2015].

3.4 Quantifying Full Variance-Covariance of Anomalous Signals

We proposed to quantify the variances and covariances in seasonal strain anomalies along with Coulomb stress changes. We now routinely use the a posteriori variances-covariances of strain rates to compute error propagation for accumulated strain, stress change and Coulomb stress changes on faults [e.g. *Kraner et al*., 2017].

3.5 Detection of large seasonal anomaly prior to South Napa Earthquake

We have extended the area of analysis to include parts of Northern California [*Kraner et al*., 2017]. We have detected a seasonal positive dilatational strain and Coulomb stress transient in the South Napa region peaking just before the 24 August 2014 M 6.0 South Napa Earthquake. Using data from 2007–2014, we show that average dilatational strain within a 500 km^2 region encompassing South Napa and northern San Pablo Bay peaks in late summer at 76±17x10^{-9} (Fig. 3a, left), accompanied by a Coulomb stress peak of 1.9 ± 0.8 kPa (Fig. 3a, right). The situation reverses in

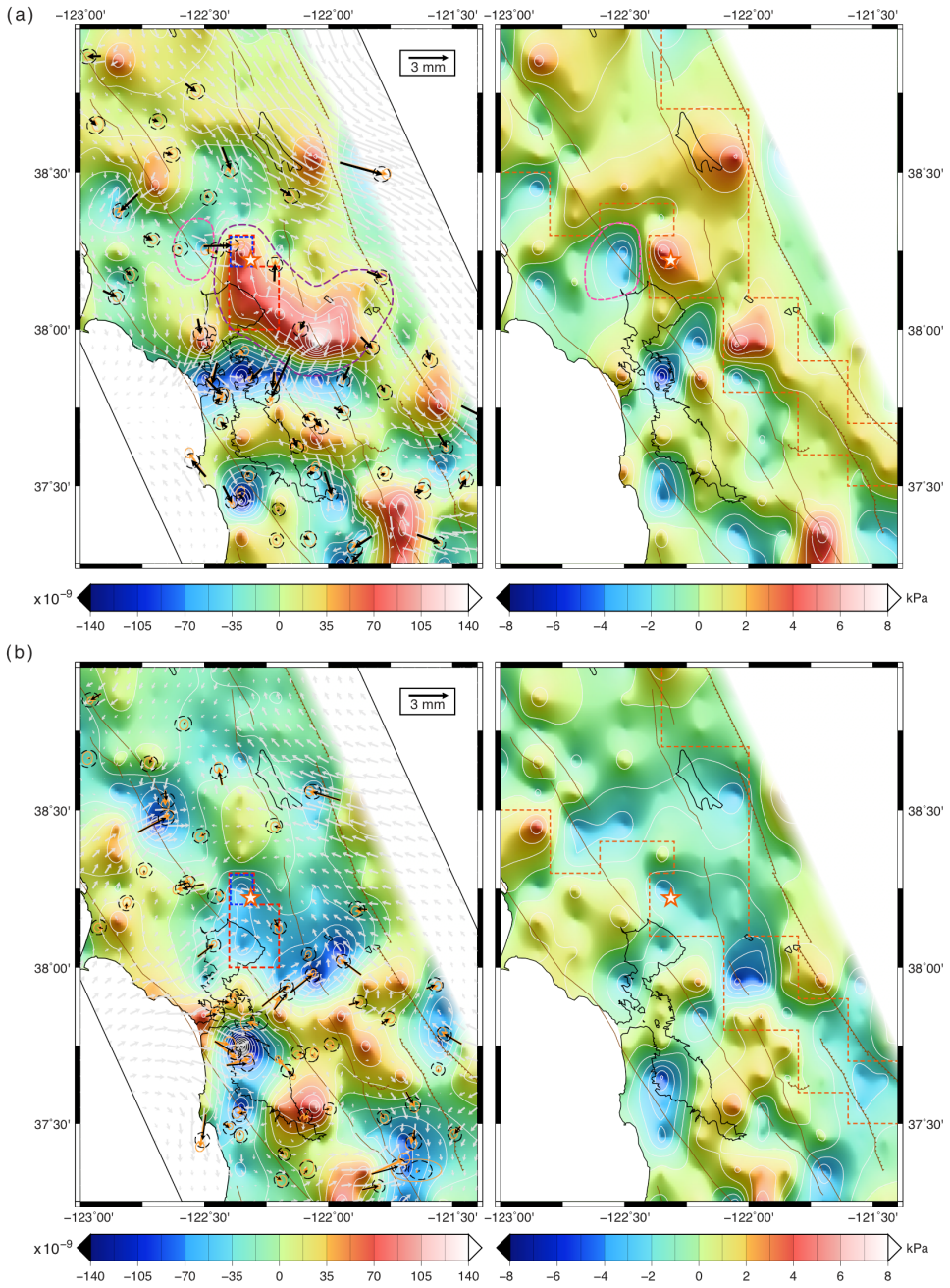

Figure 2. Stack (average) of peak yearly anomalies of dilatational strain (left) and Coulomb stress change (right) between 2007 and 2014 for summer (A) and winter (B). Orange star designates location of South Napa earthquake and brown lines show fault locations. (Left) Observed stacked measurements at cGPS stations (orange vectors), model at cGPS stations (black vectors) and model displacement field (light gray vectors) are represented. Vectors are shown with 95% confidence ellipses. Outlined areas include the 100 km^2 (blue dash) and the 500km^2 (red dash) areas where we estimate average anomalous strains and Coulomb stress changes with errors. From *Kraner et al*. (2017).

winter, with an average dilatational strain of -51 ± 37 x 10^{-9} (Fig. 3b, left) and Coulomb stress change of -1.4 ± 0.8 kPa (Fig. 3b, right). Within a smaller 100 km^2 area centered on the South Napa rupture, peak values are considerably higher, including a summer Coulomb stress peak of 5.1 ± 1.6 kPa. We examine regional seismicity but see no statistically significant correlation with seasonal Coulomb stressing in the declustered earthquake catalog (Zaliapin and Ben-Zion, 2013a,b). Using western US vertical cGPS displacements, we estimate that strain from hydrologic loading explains ≤10% of the observed long wavelength strain and only 2-3% of peak strains around the South Napa rupture. Thermoelastic crustal strain (e.g., *Berger*, 1975; *Prawirodirdjo et al.,* 2006; *Ben-Zion and Allam,* 2013) estimated from temperature gradients between the San Francisco Bay and Sacramento Valley reaches values as high as 15% of the observed strain, but the spatial strain patterns are not consistent. Vertical deformation within the Sonoma and Napa valleys inferred from InSAR explains large horizontal motions at nearby GPS stations and suggests that groundwater pumping may contribute to observed strain and stress transients in the Napa region [*Kraner et al*., 2017].

3.6 Modeling the Influence of Seasonal Transients within the Transform Plate Boundary in California

We have extended our analysis of seasonal loading to the entire plate boundary zone in California between 32.5° N – 39° N. Prior work suggests that small stress changes can influence seismicity and may contribute toward event triggering [*Heki*, 2003; *Lutrell et al*., 2007; *Bettinelli et al*., 2008; *Gonzalez et al*., 2012; *Amos et al*., 2014]. In the plate boundary wide analysis we use horizontal cGPS positions for stations in the National Science Foundation's Earthscope Plate Boundary Observatory (PBO) (Williams et al., 2010) and the University of California Berkeley Bay Area Regional Deformation Network (BARD) processed by NSF's GAGE Facility at UNAVCO, while the BARD station data are processed by University of Nevada Reno's (UNR) Geodetic Laboratory. We have quantified ten years of seasonally modulated strain history in California. We perform a higher level of damping in these solutions to suppress the shorter wavelength signals embedded in the seasonal cGPS and highlight the longer wavelength anomaly patterns. We have made animations showing the history of seasonal anomaly patterns throughout the plate boundary zone. The long-wavelength anomalies highlight remarkable seasonal periodic motions throughout much of the entire Great Valley and Sierra Nevada (Figure 3). The Mojave typically behaves opposite in dilatational strain from areas west of the San Andreas. The large-scale seasonal horizontal displacements influence the strains in parts of Northern, Central, and Southern California and produce ± 20-40 x 10^{-9} dilatational strains and Coulomb stress changes on faults of ± 1 kPa (Figure 3).

There are two important features that impact stress change, and possibly seismicity rates, on faults. During the summer and early fall, a prominent zone of dilatation and shear (involving general increase in Coulomb stress) develops along the San Andreas fault zone between 34° N – 37.5° N (Fig. 4). The Great Valley and Sierra Nevada also experience dilatational strains and displace a total of 1-2 mm toward the Great Basin during the summer-fall seasons. This pattern of periodic seasonal motion sets up particularly large shear strains in the early fall along the San Andreas fault zone between 36.5° N – 37.5° N, resulting in positive Coulomb stress changes there of more than 1 kPa (Fig. 3A, Fig. 4A,B). During winter and spring the dilatational strain patterns reverse and the Great Valley and Sierra Nevada experience compression, move 1 – 2 mm westward, and much of the San Andreas enters dilatational compression. Southern California west of the Mojave also undergoes contraction during this winter-spring time-period (Fig. 3).

Our hypothesis is that these long wavelength anomaly patterns are related to seasonal hydrologic loading [Argus et al., 2014] with the observed complexity following 2012 possibly related to draught patterns [Borsa et al., 2015]. We plan to test this by investigating the strain and displacement patterns predicted by the hydrologic loading model provided by UNAVCO. To our knowledge, our study is the first to recognize a seasonally driven pattern of increased shear and positive Coulomb stress change on the San Andreas system between 36.5° N – 37.5°N, which develops in late summer and early fall. Other regions experience periodic increases in Coulomb stress on faults that warrant further investigation. We are presently investigating seismicity rates in relation to the calculated seasonal strain anomaly patterns.

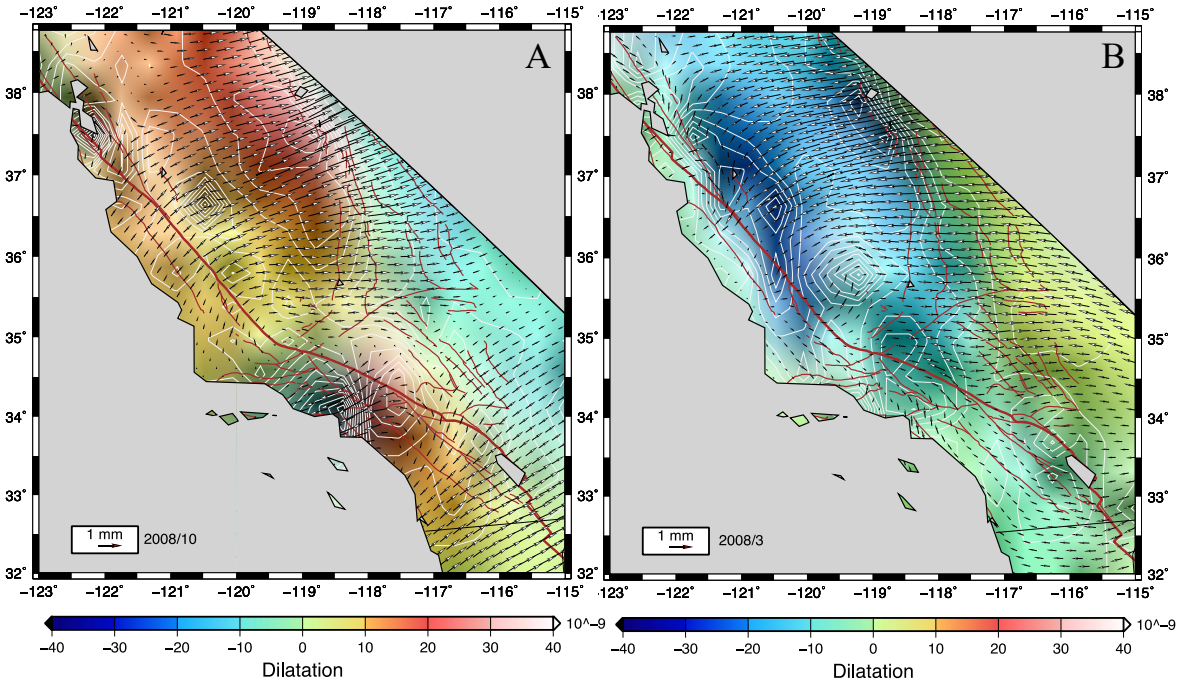

Figure 3. A. Model displacements relative to Pacific frame obtained from smoothed fit to seasonal components of CGPS data, with dilatational strains plotted in background for October, 2008, when positive dilatation dominates along parts of the San Andreas Fault and the Sierra Nevada and Great Valley displace eastward. **B**. Model displacements relative to Pacific frame for contraction period (winter), with westward motion of Great Valley and Sierra Nevada and much of San Andreas in compressional dilatational strain.

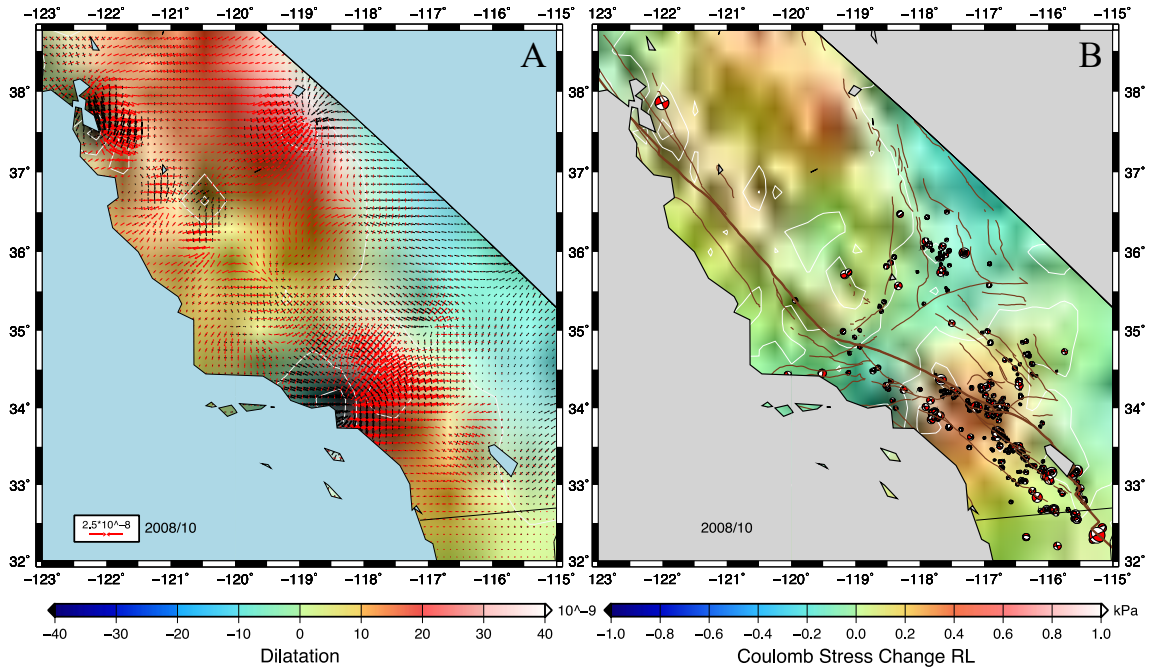

Figure 4. A. Principal strain axes (red is tensional, bold is compressional) and contoured dilatational strain corresponding to period for 10/2008 in 3A, when Sierra Nevada and Great Valley are moving eastward and large shear strain increases occur on parts of the San Andreas Fault. **B.** Coulomb stress changes on faults associated with the seasonal strain anomaly pattern in A. Note high Coulomb stress change on northern San Andreas in area of high shear. Earthquake focal mechanisms are also shown for this month.

Broader Impact. Analysis of the cGPS data have revealed significant transients on a variety of time scales. Some of these are linked with known earthquakes (post-seismic relaxation in El Mayor-Cucapah [*Pollitz et al*., 2012]; Brawly Swarm, *Hauksson et al*., 2013), whereas others are linked with unknown, and potentially slow-slip, processes (Parkfield and San Simeon regions) (Holt and Shcherbenko, 2013). We show that these anomalous strains have occurred on a variety of time scales, they involve heterogeneous distributions, and they have impacted stress rates and coulomb stress changes on faults. Current efforts are showing promise for quantifying links between measured strain changes, model stress changes, and seismicity rates. We applied the network processing tool in northern California where seasonal transient strains prior to the 2014 South Napa earthquake show a focused anomally within the South Napa region [*Kraner et al*., 2017]. The transient analysis tool has been expanded to delineate seasonal anomaly patterns throughout the entire plate boundary zone in California. This analysis has revealed seasonal large-scale periodic displacements of the Great Valley and Sierra Nevada block of ±1-2 mm, with accompanied Coulomb stress changes on sections of the San Andreas fault of ± 1kPa. We are currently developing a data product that will enable the tracking of strain and stress change evolution, along with expected seismicity rate evolution through time. The work performed to date fulfills the SCEC Science Objective 5b "*Application of geodetic detectors to the search for aseismic transients across southern California*" and also supports 2c, 1d, and 1e and 2d. Moreover, this research fulfills the recommendations under Research Strategies in Tectonic Geodesy to: (a) "*Improve our understanding of the processes underlying detected transient deformation signals and/or their seismic hazard implications through data collection and development of new analysis tools*."

3.0 Broader Impact

The Broader Impact of this work involves the training of graduate students Alireza Bahadori and Jeonghyeop Kim. The development of a data product, enabling automated detection of anomalous strain from CGPS data also constitutes a broader impact. In 2014-2015 the funding supported the training of undergraduate student Meredith Kraner. Meredith went on to graduate school at UNR and a JGR manuscript summarizing the results and method applied to the South Napa region analysis is submitted for review.

References

Amos, C.B., Audet, P., Hammond, W.C., Burgmann, R., Johanson, I.A., Blewitt, G., (2014). Uplift and seismicity driven by groundwater depletion in central California, *Nature*, 509, 483-6.

Argus, D.F., Fu, Y., and Landerer, F.W., (2014). Seasonal variation in total water storage in California inferred from GPS observations of vertical land motion, *Geophys. Res. Lett.*, 41, doi:10.1002/ 2014GL059570.

Beavan, J; Haines, J, Contemporary horizontal velocity and strain rate fields of the Pacific-Australian plate boundary zone through New Zealand, *J. Geophys. Res*., **106**, p. 741-770, 2001.

Ben-Zion, Y. and Leary, P. (1986), Thermoelastic Strain in a Half-Space Covered by Unconsolidated Material, BSSA, V. 76, No. 5, pp. 1447-1460.

Ben-Zion, Y. & A. A, Allam, (2013). Seasonal thermoelastic strain and postseismic effects in Parkfield borehole dilatometers. *Earth & Planet. Sci. Lett.* 379, 120–126, doi:10.1016/j.epsl.2013.08.024.

Berger, J. B. (1975), A Note on Thermoelastic Strains and Tilts, Jour. Geophys. Res., V. 80, No. 2, pp. 274-277.

Bettinelli, P., Avouac, J., Flouzat, M., Bollinger, L., Ramillien, G., Rajaure, S., & Sapkota, S., (2008). Seasonal variations of seismicity and geodetic strain in the Himalaya induced by surface hydrology. *Earth & Planet.Sci. Lett.* 266,332–344.

Borsa, A.A., Agnew, D.C., Cayan, D.R., (2014). Ongoing drought-induced uplift in the western United States, *Science,* 345, 1587-9.

Dieterich, J. (1994), A constitutive law for rate of earthquake production and its application to earthquake clustering, *J. Geophys. Res., 99*, 2601– 2618.

Field, E.H., et al., (2014). Uniform California Earthquake Rupture Forecast, version 3 (UCERF3)—The time-independent model, *Bull. Seismol. Soc*. Am., 104, 1122–1180, doi:10.1785/0120130164.

Freed, A. M. and R. Bürgmann (2004). Evidence of power-law flow in the Mojave desert mantle, *Nature* **430**, 548.

González, P.J., Tiampo, K.F., Palano, M., Cannavó, F. & Fernández, J., (2012). The 2011 Lorca earthquake slip distribution controlled by groundwater crustal unloading, *Nature Geosci*. 5, 821–825.

Hauksson, E., W. Yang, and P.M. Shearer (2012). "Waveform Relocated Earthquake Catalog for Southern California (1981 to 2011)"; *Bull. Seismol. Soc. Am.,* Vol. 102, No. 5, pp. –, October 2012, doi: 10.1785/0120120010.

Hauksson, E., et al. (2013), Report on the August 2012 Brawley Earthquake Swarm in Imperial Valley, Southern California, Seismol Res Lett, 84(2), 177–189, doi:10.1785/0220120169.

Heki, K., (2003). Snowload and seasonal variation of earthquake occurrence in Japan. *Earth & Planet. Sci. Lett.* 207, 159–164.

Holt, W.E., Klein, E. & Flesch, L.M., 2010. GPS strain rates, optimal fault slip rates, and predicted moment rates in Western U.S. Plate Boundary Zone, in Proceedings of the Workshop on Incorporating Geodetic Surface Deformation Data into UCERF3 Palm Spring, California.

Holt, W.E., and A.J. Haines, Velocity fields in deforming Asia from the inversion of earthquake-released strains, *Tectonics, 12*, 1-20, 1993.

Holt, W. E., N. Chamot-Rooke, X. LePichon, A.J. Haines, and J. Ren, The velocity field in Asia inferred from Quaternary fault slip rates and GPS observations, *J. Geophys. Res.*, **105**, 19185, (2000a).

Holt, W. E., B. Shen-Tu, A. J. Haines, J. Jackson, On the Determination of Self-Consistent Strain Rate Fields Within Zones of Distributed Continental Deformation, *Geophysical Monograph,* **121**, 113, (2000b).

Holt, W. E., and G. Shcherbenko (2013), Toward a Continuous Monitoring of the Horizontal Displacement Gradient Tensor Field in Southern California Using cGPS Observations from Plate Boundary Observatory (PBO), *Seism. Res. Lett., vol. 84*, No. 3, doi: 10.1785/0220130004.

Kraner, M., W. E. Holt, and A. Borsa, (2017), Tectonic Seasonal Loading Inferred from cGPS Measurements as a Potential Trigger for the M6.0 South Napa Earthquake, J. Geophys. Res., (In Review).

Lin, J., and R.S. Stein, Stress triggering in thrust and subduction earthquakes, and stress interaction between the southern San Andreas and nearby thrust and strike-slip faults, *J. Geophys. Res.*, **109**, B02303, doi:10.1029/2003JB002607, 2004.

Jennings, C. W., Fault activity map of California and adjacent areas, Cal. Dept. of Conserv., Div. of Mines and Geology, Sacramento, 1994.

Ji, K. H., and T. A. Herring (2012), Correlation between changes in ground- water levels and surface deformation from GPS measurements in the San Gabriel Valley, California,

Geophys. Res. Lett., 39, L01301, doi:10.1029/2011GL050195.

Ji, K.H., and Herring, T.A., (2013). A method for detecting transient signals in GPS position time series: smoothing and principal component analysis, *Geophysical Journal International,* 93, doi:10.1093/gji/ggt003.

King, G.C.P., R.S. Stein, and J. Lin, Static stress changes and the triggering of earthquakes, *Bull. Seismol. Soc. Amer.*, **84 (3),** 935-953, 1994.

Luttrell, K. M., X. Tong, D. T. Sandwell, B. A. Brooks, and M. G. Bevis (2011), Estimates of stress drop and crustal tectonic stress from the 27 February 2010 Maule, Chile, earthquake: Implications for fault strength, *J. Geophys. Res.*, *116*, B11401, doi:10.1029/2011JB008509.

Okada, Y. (1992), Internal deformation due to shear and tensile faults in a half-space, *Bull. Seismol. Soc. Amer.*, **82 (2)**, 1018-1040.

Mavrommatis, A.P., Segall, P., and Johnson, K.M., (2014). A decadal-scale deformation transient prior to the 2011 *Mw* 9.0 Tohoku-oki earthquake, *Geophys. Res. Lett., 41,* 4486–4494, doi:10.1002/2014GL060139.

McGuire, J. J., and P. Segall (2003), Imaging of aseismic fault slip transients recorded by dense geodetic networks*, Geophys. J. Int.* (2003) **155,** 778–788.

Pollitz, F. F., R. Bürgmann, and W. Thatcher (2012), Illumination of rheological mantle heterogeneity by the M7.2 2010 El Mayor-Cucapah earthquake, Geochem. Geophys. Geosyst., 13, Q06002, doi:10.1029/2012GC004139.

Prawirodirdjo, L., Ben-Zion, Y., and Bock, Y., (2006). Observation and modeling of thermoelastic strain in Southern California Integrated GPS Network daily position time series, *J. Geophys. Res.*, 111, B02408, doi:10.1029/2005JB003716.

Segall, P. & Matthews, M. (1997). Time dependent inversion of geodetic data, *J. Geophys. Res.,* **102,** 22 391–22 400.

Shcherbenko, G. N. (2014), Post-Seismic Strain and Stress Evolution from Continuous GPS Observations, *M.S. Thesis*, August, 1, 2014, Stony Brook University.

Shcherbenko, G., and W. E. Holt (2015). Post-Seismic Strain and Stress Evolution in southern California from Continuous GPS Observations, *In Preparation* for *Journal Geophys. Res*.

Shelly, D. R. (2009), Possible deep fault slip preceding the 2004 Parkfield earthquake, inferred from detailed observations of tectonic tremor, Geophys. Res. Lett., 36, L17318,

doi:10.1029/2009GL039589.

Shelly, D. R. Migrating tremors illuminate complex deformation beneath the seismogenic San Andreas Fault. *Nature* **463,** 648–653 (2010)

Shen-Tu, B., W. E. Holt and A. J. Haines (1999). The kinematics of the western United States estimated from Quaternary rates of slip and space geodetic data, *J. Geophys. Res,* ***104***, 28927-28955.

Shen, Z.-K., King, R. W., Agnew, D. C., Wang, M., Herring, T. A., Dong, D., Fang, P. (2011) A unified analysis of crustal motion in Southern California, 1970–2004: The SCEC crustal motion map, Journal of Geophysical Research: Solid Earth, J. Geophys. Res., 116, B11 2156-2202, http://dx.doi.org/10.1029/2011JB008549

Toda, S., R. S. Stein, K. Richards-Dinger, and S. B. Bozkurt (2005), Forecasting the evolution of seismicity in southern California: Animations built on earthquake stress transfer, J. Geophys. Res., 110, B05S16, doi:10.1029/2004JB003415.

Smith, B. R. and D. T. Sandwell (2006), A model of the earthquake cycle along the San Andreas Fault System for the past 1000 years, *J. Geophys. Res.*, *111*, B01405, doi:10.1029/2005JB003703.

Yang, W., E. Hauksson and P. M. Shearer (2012). Computing a large refined catalog of focal mechanisms for southern California (1981 - 2010): Temporal Stability of the Style of Faulting, *Bull. Seismol. Soc. Am.*, June 2012, v. 102, p. 1179-1194, doi:10.1785/0120110311.

Zaliapin, I., and Y. Ben-Zion (2013a), Earthquake clusters in southern California I: Identification and stability, J. Geophys. Res. Solid Earth, 118, 2847–2864, doi:10.1002/jgrb.50179.

Zaliapin, I., and Y. Ben-Zion (2013b), Earthquake clusters in southern California II: Classification and relation to physical properties of the crust, J. Geophys. Res. Solid Earth, 118, 2865–2877, doi:10.1002/jgrb.50178.